Contents lists available at SciOpen

Food Science and Human Wellness

journal homepage: https://www.sciopen.com/journal/2097-0765

China Food Publishing Co.

Inhibitory mechanism of CMP-LSOPC nanoparticles on advanced glycation end products release during digestion

Wenjun Li[a,1], Mengyao Niu[a,1], Chenxu Bao[a], Zihao Gong[a], Xiaozhi Ming[a], Haiyin Zheng[b], Ping Wu[b], Cui Cheng[c], Wei Li[a,*], Qian Wu[a,*]

[a] *Key Laboratory of Fermentation Engineering (Ministry of Education), National "111" Center for Cellular Regulation and Molecular Pharmaceutics, Cooperative Innovation Center of Industrial Fermentation (Ministry of Education & Hubei Province), Hubei Key Laboratory of Industrial Microbiology, Hubei University of Technology, Wuhan 430068, China*
[b] *Hubei Yizhi Konjac Biotechnology Co., Ltd., Yichang 443300, China*
[c] *Hubei Yanqi Biotechnology Co., Ltd., Xiangyang 441200, China*

ARTICLE INFO

Article history:
Received 28 July 2024
Received in revised form 9 September 2024
Accepted 16 December 2024

Keywords:
Advanced glycation end products
Gastrointestinal digestion
Enzyme inhibition
Lotus seedpod oligomeric procyanidins
Carboxymethyl pachymaran

ABSTRACT

Advanced glycation end products (AGEs) are harmful molecules formed through non-enzymatic reactions between proteins, lipids, and reducing sugars, contributing to diseases such as diabetes, Alzheimer's disease, and cardiovascular conditions. This study investigates the inhibitory mechanisms of CMP-LSOPC nanoparticles (NPs) on AGEs release during gastrointestinal digestion. CMP-LSOPC NPs were synthesized by complexing carboxymethyl pachymaran (CMP) with lotus seedpod oligomeric procyanidins (LSOPC), and its structure confirmed *via* Fourier transform infrared (FTIR), ultraviolet-visible (UV-Vis), scanning electron microscopy (SEM), and differential scanning calorimetry (DSC) analyses. In simulated gastrointestinal conditions, CMP-LSOPC NPs exhibited a significant reduction in AGE formation, achieving up to lowering AGE release by 48.5% compared to LSOPC alone. Furthermore, associated mechanisms are explored, including CMP-LSOPC NPs improving the stability and antioxidant activity of LSOPC, inhibiting the activity of related hydrolase enzymes in the gastrointestinal environment. The CMP-LSOPC NPs exhibited 4.1% higher LSOPC content during the gastric phase compared to LSOPC alone, indicating that CMP-LSOPC NPs with better stability. The antioxidant activity, measured through DPPH, $ABTS^{+}$, and hydroxyl radical scavenging assays, demonstrated that CMP-LSOPC NPs enhanced antioxidant capacity, with a 35% increase in DPPH radical scavenging and 29% increase in $ABTS^{+}$ radical scavenging compared to LSOPC alone. Enzyme inhibition assays showed a protective effect, with a 22% decrease in trypsin activity and 19% reduction in pepsin activity. Meanwhile, mass spectrometry revealed the presence of more long-chain glycopeptides in the CMP-LSOPC NPs group, which may exert beneficial influence on adiminishing the absorption of harmful AGEs. However, the potential risks of accumulating long glycated peptides in the colon should not be overlooked. Overall, CMP-LSOPC NPs effectively inhibited AGE release, which may offer a promising strategy for reducing the dietary risk of AGEs.

1. Introduction

Advanced glycation end products (AGEs) are stable substances formed through the non-enzymatic reaction of proteins, lipids, and other macromolecules with glucose or reducing monosaccharides. These reactions can occur endogenously or during the processing of food[1]. AGEs are potent cytotoxic molecules that promote host cell death and organ damage[2]. They accumulate in the extracellular matrix of various tissues, causing structural and functional damage to organisms[3]. AGEs not only trigger the onset of complications associated with diabetes[4], but also contribute to the pathogenesis of numerous diseases, including Alzheimer's disease (AD)[5], Parkinson's disease (PD), renal failure[6], liver damage, atherosclerosis, cerebrovascular diseases and cancer[7].

Inhibition of AGEs formation is currently a major area of research interests[8]. While drugs including aminoguanidine, metformin, and

[1] These authors contributed equally.

* Corresponding authors at: School of Life and Health Sciences, Hubei University of Technology, Wuhan 430068, China.
Email address: wesley@hbut.edu.cn (W. Li); wuqian@hbut.edu.cn (Q. Wu)

Peer review under responsibility of Beijing Academy of Food Sciences.

SciOpen Publishing services by Tsinghua University Press

http://doi.org/10.26599/FSHW.2025.9250481

pioglitazone, can suppress AGE formation[9], they have side effects such as nausea and diarrhea. Current researches focus on natural substances like polyphenols[10] and polysaccharides[11], which can inhibit AGEs during food processing but cannot fully eliminate them without affecting flavor. Consequently, AGEs are absorbed during digestion, necessitating inhibition during this phase to prevent them from reaching target organs and triggering inflammation and disease.

Lotus seedpod oligomeric procyanidin (LSOPC), with its susceptibility to degradation and ability to inhibit AGEs formation, is prone to gastrointestinal degradation. Encapsulation with polysaccharides is an effective method to enhance the gastrointestinal stability of polyphenols. *Poria cocos* is an important "medicine food homology" plant in China. With advancing research, the antioxidant, anti-tumor, anti-inflammatory, and immune-boosting activities of *P. cocos* polysaccharides have been validated and applied both *in vitro* and *in vivo*[12]. The water-insoluble and alkali-soluble *P. cocos* polysaccharides, after carboxymethylation to form carboxymethyl pachymaran (CMP), demonstrate enhanced solubility and biological activity.

This study prepares CMP-LSOPC nanoparticles (CMP-LSOPC NPs). The primary focus of the study is to investigate the improvement of LSOPC's stability in simulated gastrointestinal environments, and to explore the efficacy of CMP-LSOPC NPs as exogenous additives in inhibiting the release of AGEs during the digestion of glycated proteins. The relevant mechanism will lay solid foundations for the subsequent studies on absorption and metabolism of peptide-AGEs.

2. Materials and methods

2.1 Main materials and reagents

CMP (≥ 85%) and LSOPC (≥ 85%) were both prepared internally in the laboratory. Lactose (containing 70% *β*-lactose and 30% *α*-lactose) and pepsin (≥ 3 000 U/g) were acquired from Shanghai Macklin Biochemical Co., Ltd. (Shanghai, China). Trypsin (≥ 4 000 U/g) and porcine bile salts were procured from Shanghai Yuan Ye Biological Technology Co., Ltd. (Shanghai, China). Casein (98%) was purchased from Sigma-Aldrich (Shanghai, China).

2.2 Synthesis of CMP-LSOPC NPs

It has previously investigated the effects of different temperature, time, and dosage ratios on the binding of anthocyanins to CMP to form complexes[11-13]. The optimized treatment was obtained after single factor experiments and orthogonal design, where CMP was mixed with LSOPC at a ratio of 1.00:4.35 (*m*/*m*) at 40 ℃ for 4 h. In detail, CMP and LSOPC mixture was stirred until complete dissolution of the sample was achieved, followed by the incubation at 40 °C for 4 h using an electric thermostatic water bath (Beijing Chang'an Scientific Instrument Factory, Beijing, China). A portion of the solution was set aside as the non-homogenized CMP-LSOPC complex. The remaining complex solution was dispersed for 5 min at 8 000 r/min using a high-speed disperser, and then homogenized 3 times at 10 000 Psi using a high-pressure nano homogenizer to prepare CMP-LSOPC NPs.

Both complex solutions were transferred into pre-treated dialysis bags (molecular weight cut-off of 3 500 Da) and the reaction temperature was maintained at 40 °C. Dialysis was continued until adsorption equilibrium was reached, indicated by a constant absorbance of the free oligomeric procyanidins at 280 nm outside the dialysis bag. The homogenized complex solution was then filtered through a 420 nm pore size membrane filter, and the resulting product was freeze-dried to obtain CMP-LSOPC NPs.

2.3 Loading efficiency and loading capacity of LSOPC in the complexes

The total LSOPC content of the pre-lyophilization complex samples prepared in Section 2.2 was quantitatively determined using the 4-dimethylaminocinnamaldehyde (DMAC) method[14]. This procedure was utilized to compare the effects of nanoparticle formation on the loading efficiency and loading capacity. A 0.1% DMAC solution was prepared before using (solvent composed of ethanol:water:HCl = 75.0:12.5:12.5). Samples were mixed with the DMAC solution at a 1:3 (*V*/*V*) ratio, thoroughly vortexed, and reacted at room temperature for 15 min. The absorbance was then read at 640 nm. The blank group utilized ethanol in place of the sample, and the control group did not include the DMAC solution. The total oligomeric procyanidins concentration in the samples was quantified using a standard curve derived from a procyanidin standard. The loading efficiency and loading capacity were calculated using the formulas (1)–(2) [15], with values expressed as the mean of repeated analyses.

$$\text{Loading efficiency (\%)} = \frac{A_0 - A_1}{A_0} \times 100 \quad (1)$$

$$\text{Loading capacity (mg/mg)} = \frac{A_0 - A_1}{A_2} \quad (2)$$

Where A_0 (mg) is the amount of LSOPC added to the system; A_1 (mg) is the amount of LSOPC in the filtrate; A_2 (mg) is the total amount of the complex.

2.4 Identification of LSOPC components

The LSOPC content was determined according to the method reported by the previous study[16]. LSOPC, obtained by lyophilization, was reconstituted in 50% methanol aqueous solution and filtered through a 0.22 μm organic phase filter membrane prior to analysis. LSOPC was identified using a Thermo Scientific Q-Exactive high-resolution liquid chromatography-mass spectrometry (LC-MS) system (Thermo Fisher Scientific, Waltham, MA, USA).

Chromatographic conditions were as follows: The column was a Diamonsil TM-C_{18} column (4.6 × 200.0 mm, 5 μm); column temperature was maintained at 35 °C; mobile phase consisted of 0.1% formic acid in water (solvent A) and acetonitrile (solvent B). The elution gradient was set as 4%–20% B from 0 to 3 min; held at 20% B from 3 to 6 min; 20%–30% B from 6 to 12 min; and 30%–75% B from 12 to 24 min; followed by a 10 min column re-equilibration. The flow rate was set at 500 μL/min with an injection volume of 10 μL.

Mass spectrometry was performed in the negative ionization mode. The electrospray ionization (ESI) source operating parameters were as follows: fragment voltage of 70 V, capillary voltage of 3 000 V, sheath gas flow rate of 12 mL/min, aux gas heater temperature at 300 °C, and a nebulizer pressure of 40 psi. Nitrogen was used as the auxiliary gas.

The mass spectral ion scanning range was set from *m*/*z* 100 to 1 500 with concurrent secondary fragmentation.

2.5 Analytical characterization methods for CMP-LSOPC NPs

2.5.1 Nanoparticle size and Zeta potential

Prior to freeze-drying, the CMP-LSOPC NPs samples were diluted with deionized water to an appropriate degree to circumvent multiple scattering effects. Particle size and Zeta potential were measured using a nanoparticle size and Zeta potential analyzer to compare the impact of nanoparticle formulation on these parameters[17].

2.5.2 Impact of CMP on the thermal stability of LSOPC

For the thermal effect analysis, 10mg LSOPC, CMP, and CMP-LSOPC NPs were placed into aluminum pans and compacted. The samples were then heated from 50 to 300 °C at a rate of 10 °C/min under nitrogen protection, with an empty aluminum pan serving as a reference to obtain the differential scanning calorimetry (DSC) thermograms for each substance. By comparing the thermograms of the isolated LSOPC and CMP with that of the CMP-LSOPC NPs, the changes in the endothermic and exothermic peaks across the DSC curves were analyzed[18].

2.5.3 Impact of structural characteristics of CMP-LSOPC NPs on the functional properties

The Fourier-transform infrared (FTIR) spectroscopy was used to analyze the molecular interactions and chemical bonds in the CMP-LSOPC NPs, using a Nexus 470 FTIR spectrometer (Thermo Nicolet, USA)[19]. The attenuated total reflectance (ATR) technique was employed, placing the sample directly on the surface of the ATR crystal for analysis. The spectrometer was configured to conduct a full-waveband scan covering the range of 4 000–400 cm^{-1}, with the number of scans set at 25 and a resolution of 4 cm^{-1}. Each sample underwent 3 parallel measurements to ensure the accuracy of the results. A blank ATR crystal was used as the background, conducting 32 scans to obtain a stable background spectrum, which was then averaged for correction. The infrared spectral data of the samples were processed using OMNIC software version 8.2 (Thermo Fisher Scientific Inc., MA, USA).

The ultraviolet (UV) spectroscopy was used to investigate the UV absorption characteristics of polyphenols and polysaccharides, providing information on the absorption of these small molecules at specific wavelengths. This method is effectively utilized to study the interactions between polyphenols and polysaccharides and any potential conformational changes[20]. Lyophilized CMP-LSOPC NPs powder, LSOPC, and their monomers were dissolved in buffer solution (pH 7.4, 0.2 mol/L PBS, 2.7 mmol/L KCl, 137 mmol/L NaCl). The CMP-LSOPC NPs solution was mixed proportionally with the LSOPC and its monomer solutions and incubated at 37 °C for 1 h. The absorption spectra of each sample group within the wavelength range of 190 to 400 nm were measured using a UV-1601 ultraviolet-visible (UV-Vis) spectrophotometer (Beijing Rayleigh Analytical Instrument Co., Beijing, China), with the buffer serving as the reference. Three measurements were conducted for each sample.

Scanning electron microscopy (SEM) was used to analyze the microstructure and surface morphology. The lyophilized samples of LSOPC, CMP, and CMP-LSOPC NPs were evenly spread on a carrier platform coated with conductive adhesive. After gold sputter coating under vacuum conditions, the samples were observed using a scanning electron microscope (Hitachi S3400N, Japan). The operational voltage was set at 15 kV, and the microstructure and surface morphology of the samples were observed at various magnifications.

2.6 Inhibitory effects of CMP-LSOPC NPs on AGEs release during gastrointestinal digestion

Simulated salivary fluid (SSF), simulated gastric fluid (SGF), and simulated intestinal fluid (SIF) electrolyte stock solutions were prepared using the corresponding electrolytes[21]. A glycated protein model system was created using lactose and casein. Sample treatment was divided into 3 groups: the sample for the CMP-LSOPC NPs group was prepared according to the Section 2.2, the ratio of LSOPC to CMP was 1.00:4.35 (*m*/*m*), then weighing equivalent CMP or LSOPC to establish the CMP group and the LSOPC group, respectively. The gastrointestinal digestion was simulated following the method of Minekus et al.[22].

The mass of LSOPC and CMP was selected based on the loading amount of the nanocomposite, with a mass ratio of 1.00:4.35, to ensure that the concentrations of the polysaccharide and polyphenol groups were equivalent to the concentration of the original procyanidins and CMP in the complex. The fluorescence intensity of fluorescent AGEs was monitored using an F-4700 fluorescence spectrophotometer (Hitachi, Japan) with an excitation wavelength of 370 nm, emission wavelength of 440 nm, and slit width of 5 nm for both excitation and emission at a voltage of 700 V. The relative inhibitory rate was calculated using the following formula (3):

$$\text{Relative inhibitory rate (\%)} = \frac{F_{\text{control}} - F_{\text{sample}}}{F_{\text{control}}} \times 100 \quad (3)$$

Where F_{sample} is the fluorescence value of the digestive fluid with the sample added; F_{control} is the fluorescence value of the digestive fluid without the sample added.

2.7 Inhibition mechanism of CMP-LSOPC NPs on AGEs release during digestion

2.7.1 Antioxidant activity of digestive fluids

2.7.1.1 DPPH radical scavenging activity

The gastrointestinal digesta, diluted to an appropriate degree, were mixed with a DPPH ethanol solution (0.1 mmo/L) and stored in the dark for 0.5 h. The absorbance was measured at 517 nm using a UV-Vis spectrophotometer[23]. The formula (4) for the DPPH radical scavenging rate is:

$$\text{DPPH radical scavenging rate (\%)} = \frac{1 - (A - A_b)}{A_0} \times 100 \quad (4)$$

Where A is the absorbance of the digesta post-reaction with DPPH containing the LSOPC/CMP/CMP-LSOPC NPs/CMP + LSOPC

mixture; A_0 is the absorbance of DPPH; A_b is the absorbance of the digesta containing LSOPC/CMP/CMP-LSOPC NPs.

2.7.1.2 $ABTS^+$ radical scavenging activity

$ABTS^+$ radicals were prepared by mixing ABTS solution (7.4 mmol/L) with $K_2S_2O_8$ solution (2.6 mmol/L) and allowed to react in the dark at room temperature for 12 h before measurement. The $ABTS^+$ solution was then diluted to an absorbance of approximately 0.70 ± 0.02 at 734 nm. The gastrointestinal digesta, diluted to an appropriate degree, were mixed with the $ABTS^+$ solution and stored at room temperature for 6 min. The absorbance was measured at 734 nm using a spectrophotometer[24]. The formula (5) for the $ABTS^+$ radical scavenging rate is:

$$\text{ABTS}^+ \text{ radical scavenging rate (\%)} = \frac{A_0 - A}{A_0} \times 100 \quad (5)$$

Where A is the absorbance of the sample containing $ABTS^+$; A_0 is the absorbance of $ABTS^+$.

2.7.1.3 Hydroxyl radical scavenging activity

The gastrointestinal digesta, diluted to an appropriate degree, were mixed with 9 mmol/L $FeSO_4$ and 8.8 mmol/L H_2O_2 maintained at 20 °C for 10 min, followed by the addition of the 9 mmol/L salicylic acid-ethanol solution. The absorbance was measured at 510 nm using a spectrophotometer[25]. The formula (6) for the hydroxyl radical scavenging rate is given by:

$$\text{Hydroxyl radical scavenging rate (\%)} = \left(1 - \frac{A_0 - A}{A_0}\right) \times 100 \quad (6)$$

Where A_0 is the absorbance of the sample replaced by H_2O; A_1 is the absorbance of the sample; A_2 is the absorbance of the sample after replacing H_2O_2 with H_2O.

2.7.2 Inhibition of enzyme activity by CMP-LSOPC NPs

2.7.2.1 Preparation and assessment of enzyme activity samples

Enzyme activity samples were prepared in accordance with the LSOPC to CMP binding ratio of 1:4.35, ensuring that the concentrations of LSOPC and CMP in the CMP group and LSOPC group were identical to those in the CMP-LSOPC NPs group. The inhibitory capacity of the samples on pepsin enzyme activity was determined following the method of Petrat-Melin et al.[26], while the inhibitory capacity on trypsin enzyme activity was measured according to Gonçalves et al.[27].

2.7.2.2 Interactions between LSOPC, pepsin/trypsin, and glycated proteins

FTIR spectroscopy: pepsin, trypsin, and glycated proteins were each dissolved in phosphate buffer solutions (50 mmol/L) at the corresponding pH conditions (pH 2.0 or pH 7.0) to the final concentration of 1 mg/mL. LSOPC, CMP, and CMP-LSOPC NPs were added to the aforementioned solutions, thoroughly mixed, heated in a 37 °C water bath for 30 min followed by lyophilized. The lyophilized samples were placed directly onto the ATR crystal for FTIR spectral analysis using a Nexus 470 FTIR spectrometer, with an average of 32 scans to obtain the FTIR spectra of the samples. The scanning range was set from 4 000 to 400 cm^{-1} with a resolution of 4 cm^{-1}. OMNIC and Matplotlib software were used for further processing of the infrared spectral data.

SEM: The surface morphology of the freeze-dried samples, illustrating the interactions between CMP-LSOPC NPs with glycated casein substrate (G-CS) and digestive enzymes, was observed using SEM as described in Section 2.5.3.

2.7.3 LSOPC remaining rate detection

A total of 2 mL of digesta were extracted 3 times with ethyl acetate, collected in a rotary flask, and the ethyl acetate phase was removed under reduced pressure. The proanthocyanidins were then redissolved in deionized water. The content of proanthocyanidin monomers in the digestion samples was calculated using external standard curves of their respective standards. The total proanthocyanidin content was accurately quantified using the DMAC method[14].

2.7.4 Oligopeptide mass spectrometry identification

The oligopeptides of LSOPC were prepared by modifying the method reported by Kong et al.[28]. The digestive fluids obtained post gastrointestinal digestion were transferred into a 10 kDa ultrafiltration tube. After centrifugation at 14 000 × *g* for 15 min, the filtrate was collected as the undigested protein solution. The filtrate was then transferred to a 200 Da molecular weight dialysis bag, with water being changed every 12 h for 24 h. Then the retention solution after, was freeze-dried and stored at –20°C.

The desalted water samples, obtained *via* LC separation, were directly injected into a mass spectrometer. Proteins and peptides were analyzed using LC-MS^2 (Eksigent micro-LC; AB Sciex TripleTOF 5600-plus). The protein solution was subjected to gradient elution on a C_{18} extraction column (100 μm × 20 mm, 5 μm) with a flow rate of 5 μL/min on a C_{18} analytical column (300 μm × 150 mm, 3 μm). The gradient elution lasted for 30 min with the following solvents: Solution A (2% acetonitrile + 0.1% formic acid + 98% H_2O); Solution B (98% acetonitrile + 0.1% formic acid + 2% H_2O). The 30 min elation program was as follows: 0 min, 5% B; 5 min, 5%–35% B; 1 min, 35%–55% B; 1 min, 55%–5% B. The LC gradient elution was controlled at a constant temperature with the Triple TOF 5600 plus mass spectrometer. The spray heater temperature was set to 50 °C, and the corona discharge needle voltage was 2.2 kV. The mass spectrometer was set to scan ions in the range of *m*/*z* 350–1 500 for MS^1 and *m*/*z* 100–1 500 for MS^2. Singly charged ions were excluded, with a resolution setting of 1.6 Da. MS^1 scans had a resolution of 30 000 and MS^2 scans had a resolution of 15 000. The normalized collision energy was set to 28, with a dynamic collision energy adjustment range of 2 × 10^5. The precursor ion dynamic exclusion time was 10 s. MS^1 scans were performed with a 250 ms scan window, and MS^2 scans of 25 precursor ions were performed with a 100 ms scan window.

Protein and peptide identification were performed using the Mascot Daemon database search program to analyze the MS and MS² data of the complex mixtures.

2.8 Data analysis

Data were analyzed using SciPy stats version 1.13.1 in Python 3.9.13, and differences were considered statistically significant at $P < 0.05$. The statistical analyses mainly included descriptive statistics and *t*-tests. Figures were created using Matplotlib 3.8.2. Please remove "R", as the final data analysis results presented in the manuscript were mainly based on SciPy stats and Matplotlib visualization.

3. Results and discussion

3.1 Composition of LSOPC

The LSOPC was identified using LC-MS/MS in negative ion mode, revealing 4 flavanol monomers, 10 procyanidin dimers, 4 procyanidin trimers, 2 dihydroflavonols, and 2 dihydroflavonol-*O*-glycosides (Fig. 1). High-resolution mass spectrometry data for these compounds are summarized, including retention time (tR in minutes), calculated and observed parent ion masses (*m*/*z*), molecular formula, and identified compositions (Table 1).

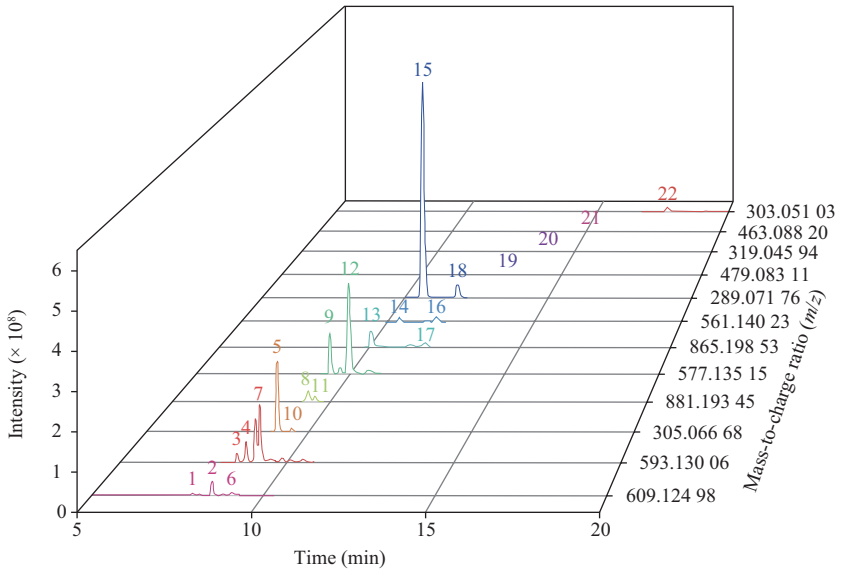

Fig. 1 Chromatogram of LSOPC as identified by LC-MS/MS in the negative ion mode.

Table 1
High-resolution mass, molecular weight, error, and fragment ions of all compounds identified in LSOPC.

No.	Retention time (min)	Theoretical ion mass (*m*/*z*)	Molecular formula	Identification
1	7.92	609.124 98	$C_{30}H_{26}O_{14}$	EG-EG
2	8.48	609.124 98	$C_{30}H_{26}O_{14}$	EG-EG
3	8.50	593.130 06	$C_{30}H_{26}O_{13}$	EG-EG
4	8.77	593.130 06	$C_{30}H_{26}O_{13}$	EG-EG
5	9.00	305.066 68	$C_{15}H_{14}O_{7}$	GC
6	9.07	609.124 98	$C_{30}H_{26}O_{14}$	EG-EG
7	9.11	593.130 06	$C_{30}H_{26}O_{13}$	EG-EG
8	9.29	881.193 45	$C_{45}H_{38}O_{19}$	EG-EC-EC
9	9.32	577.135 15	$C_{30}H_{26}O_{12}$	EC-EC
10	9.43	305.066 68	$C_{15}H_{14}O_{7}$	EGC
11	9.50	881.193 45	$C_{45}H_{38}O_{19}$	EC-EC-EG
12	9.93	577.135 15	$C_{30}H_{26}O_{12}$	EC-EC
13	10.04	865.198 53	$C_{45}H_{38}O_{18}$	EC-EC-EG
14	10.47	561.140 23	$C_{30}H_{26}O_{11}$	EA-EC
15	10.62	289.071 76	$C_{15}H_{14}O_{6}$	CC
16	11.65	561.140 23	$C_{30}H_{26}O_{11}$	EA-EC
17	11.84	865.198 53	$C_{45}H_{38}O_{18}$	EC-EC-EC
18	11.91	289.071 76	$C_{15}H_{14}O_{6}$	EC
19	13.10	479.083 11	$C_{21}H_{20}O_{13}$	Myricetin-3-*O*-glucoside
20	14.05	319.045 94	$C_{15}H_{12}O_{8}$	Dihydromyricetin
21	15.21	463.088 20	$C_{21}H_{20}O_{12}$	Quercetin3-*O*-glucoside
22	17.80	303.051 03	$C_{15}H_{12}O_{7}$	Dihydroquercetin

The results revealed the presence of a diverse array of flavan-based compounds in LSOPC, including flavanol monomers, procyanidin dimers and trimers, as well as dihydroflavonol and its glycoside derivatives. These compounds were structurally identified through specific cleavage patterns and neutral losses, such as QM cleavage, Retro RDA fragmentation and HRF. Specifically, compounds 1, 2, and 6 were identified as procyanidin dimers containing 2 EG units; compounds 3, 4, and 7 were determined to be procyanidin dimer isomers comprising EG and EC units; compounds 8 and 11 were inferred to be procyanidin trimers formed by 2 EC units and one EG unit; compounds 9 and 12 were identified as B-type procyanidin dimers; compounds 19, 20, 21, and 22 were respectively identified as gallocatechin-3-*O*-glucoside, dihydromyricetin, quercetin-3-*O*-glucoside, and dihydroquercetin.

3.2 Characterization of CMP-LSOPC NPs

The particle size distribution of CMP-LSOPC NPs varies in volume percentage from 100 to 1 000 mm. Initially, the volume percentage increases with particle size, peaking at approximately 13%, then decreases as the particle size continues to increase. This indicates a higher concentration tendency within a specific size range but shows overall size distribution non-uniformity (Fig. 2A). As shown in Table 2, the average particle size of CMP-LSOPC NPs without homogenization (homogenization cycle 0) was (1 726.23 ± 91.91) nm, with a polydispersity index (PDI) of 0.90 ± 0.18 and a Zeta potential of (–42.00 ± 4.00) mV. After 3 cycles of homogenization, the average particle size significantly decreased to (244.83 ± 1.60) nm, PDI dropped to 0.22 ± 0.01, and the Zeta potential reduced to (–52.67 ± 2.66) mV. These results suggest that the solute particle size became uniform, and the system more stable after homogenization. The changes in particle size and Zeta potential indicate a successful complexation between LSOPC and CMP[29].

Table 2
Average particle size, PDI, and Zeta potential of CMP-LSOPC NPs.

Homogenization cycles	Size (nm)	PDI	Zeta Potential (mV)
0	1 726.23 ± 91.91	0.90 ± 0.18	–42.00 ± 4.00
3	244.83 ± 1.60	0.22 ± 0.01	–52.67 ± 2.66

The loading efficiency and capacity of CMP-LSOPC NPs are significantly higher than those of CMP-LSOPC (Table 3). This may be attributed to the larger specific surface area and volume ratio of the nanostructure, which enables binding to a greater number of small molecules. This suggests that the preparation of the complex into nanoparticles is more conducive to the combination of CMP and LSOPC.

The FTIR spectrum indicates a distinct hydroxyl absorption peak for LSOPC at 3 278 cm^{-1} (Fig. 2B), along with characteristic absorption peaks of aromatic rings at 1 604, 1 515, and 1 445 cm^{-1}. CMP shows a hydroxyl absorption peak at 3 278 cm^{-1}, a C–H stretching vibration absorption peak at 2 919 cm^{-1}, 2 characteristic peaks at 1 585 and 1 421 cm^{-1} corresponding to asymmetric and symmetric stretching vibrations of the carboxylate COO– group, a C–N stretching vibration at 1 322 cm^{-1}, and a C–O stretching vibration absorption peak at 1 058 cm^{-1}. The CMP-LSOPC NPs spectrum also displays these characteristic peaks, but with peak positions being shifted. The hydroxyl stretching vibration peak of the complex repositions to 3 354 cm^{-1}, indicating a blue shift of the hydroxyl peak, which suggests hydrogen bond interactions as well as possible van der Waals forces between CMP and LSOPC[30]. Additionally, compared to LSOPC, the characteristic absorption peaks of aromatic rings in CMP-LSOPC NPs disappear, and more features similar to CMP appear, possibly due to the formation of aggregates between LSOPC and CMP, obscuring characteristic peaks.

Table 3
Loading efficiency and loading capacity of LSOPC in the complexes.

Complexes	Loading efficiency (%)	Loading capacity (mg/mg)
CMP-LSOPC	83.96 ± 3.46	0.17 ± 0.01
CMP-LSOPC NPs	94.63 ± 0.69	0.19 ± 0.01

The UV spectrum displays a red shift and increased intensity of the maximum absorption peak of CMP-LSOPC NPs (Fig. 2C), indicating structural changes in LSOPC under the influence of CMP, suggesting successful complexation. It is hypothesized that LSOPC and its monomers may interact with CMP, reducing the electronic excitation energy of the chromophores in aromatic amino acid residues. This could further alter the hydrogen bonds between aromatic amino acid residues (tyrosine) and solvent molecules, leading to a change in the maximum absorption wavelength of CMP-LSOPC NPs.

The microstructures of LSOPC, CMP, and CMP-LSOPC NPs, as shown in Fig. 2D, reveal that LSOPC exhibits irregular flaky crystals with a porous surface, likely due to internal moisture evaporation during freeze-drying. CMP generally presents a flaky structure with a dense and rough surface. These characteristics provide them with a large specific surface area, enabling effective adsorption and fixation of a significant amount of LSOPC molecules[31]. CMP-LSOPC NPs display a film-like structure with various tendrils and holes of different sizes.

Fig. 2E shows the results of thermal stability of nanoparticles as detected by DSC. Unlike CMP and the complex, LSOPC's DSC curve shows 2 peaks at 73.2 and 99.0 °C, potentially due to hydroxyl oxidation on different rings and dehydration of the proanthocyanidin sample. The decomposition peak of carboxymethyl groups occurs between 230–260 °C, where carboxymethyl groups undergo cleavage, releasing carboxyl and carbonyl groups. The exothermic peak area of the complex group at 239 °C is smaller than that of the CMP group, possibly due to some carboxymethyl groups being obscured by the combination of LSOPC and CMP. The complexation leads to an increase in the recrystallization temperature and a reduction in the exothermic peak area, further confirming the successful complexation of the samples.

3.3 Inhibitory effect of CMP-LSOPC NPs on AGEs formation during gastrointestinal digestion

Inhibitory rates of AGEs during the gastrointestinal digestion are shown in Fig. 3. During the gastric digestion phase, the CMP-LSOPC NPs group exhibited a higher inhibition rate of AGEs, indicating that complexation enhanced the stability of LSOPC in gastric digestion. In the intestinal digestion phase, the inhibition rate of the CMP-LSOPC NPs group decreased, which is attributed to the lower release rate of LSOPC in the intestinal stage. The overall inhibition rate during the gastric phase was higher than that in the intestinal phase, possibly because polyphenols exhibit stronger antioxidant activity in acidic environments, a finding that aligns with Wu et al.[32]. Furthermore, polysaccharides tend to undergo the Maillard reaction with proteins in alkaline environments. While complexation may not exhibit superior inhibitory activity compared to LSOPC alone in the early stages of digestion, our results show that CMP-LSOPC NPs demonstrate better stability and inhibitory effects from 3 h onward.

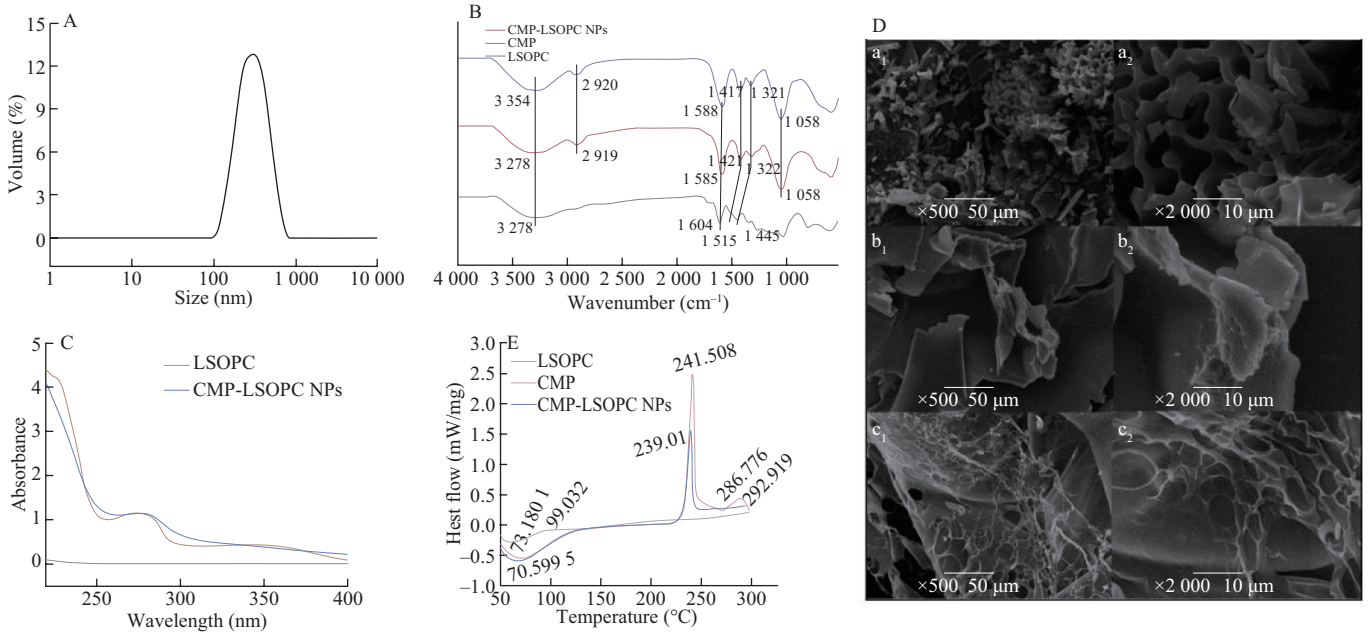

Fig. 2 Characterization results of CMP-LSOPC NPs. (A) Particle size distribution of CMP-LSOPC NPs; (B) FTIR spectroscopy spectra; (C) UV-Vis absorption spectra; (D) Results of SEM analysis (a, LSOPC; b, CMP; c, CMP-LSOPC NPs); (E) outcomes of DSC analysis.

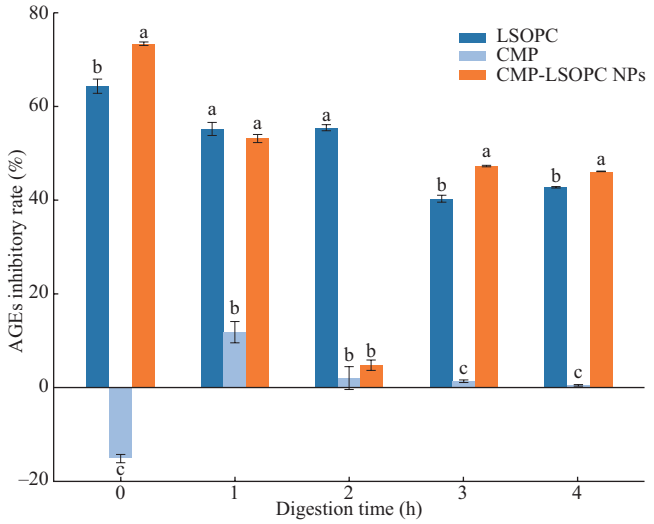

Fig. 3 AGEs inhibition rates in the gastric and intestinal digestion of CMP, LSOPC, and CMP-LSOPC NPs. Different lowercase letters indicate significant differences ($P < 0.05$).

3.4 Inhibitory mechanism of gastrointestinal release of AGEs by CMP-LSOPC NPs

3.4.1 Antioxidant properties of simulated gastrointestinal digestive fluids

As illustrated in Fig. 4, CMP-LSOPC NPs significantly enhance the antioxidant capacity of digestive fluids. During the gastric digestion phase (Fig. $4A_1$), the DPPH radical scavenging rate of the LSOPC group was higher than that of the CMP-LSOPC NPs groups. This could be due to the tight binding of LSOPC and CMP within CMP-LSOPC NPs during gastric digestion, which better protects LSOPC, leading to a higher retention rate of LSOPC in the CMP-LSOPC NPs group during intestinal digestion. This results in the release of more LSOPC, thereby enhancing the antioxidant activity of the digestive fluid.

In the $ABTS^+$ assay group, there was a clear trend in the overall antioxidant performance (Fig. $4B_2$). Under simulated intestinal fluid conditions, the CMP-LSOPC NPs group exhibited superior antioxidant capabilities. This result reflects the protective effect of the complex on antioxidant properties.

As shown in Fig. $4C_1$, CMP-LSOPC NPs significantly improve the antioxidant capacity of the digestive fluid. During the gastric digestion phase, the hydroxyl radical scavenging rate of the LSOPC groups was lower than that of the CMP and CMP-LSOPC NPs group, possibly due to the complexation of LSOPC with CMP in the gastric phase, which masks the active groups of LSOPC. The antioxidant properties of the intestinal digesta of the complex group were better, consistent with results found by Wu et al.[33].

3.4.2 Effects of CMP-LSOPC NPs on digestive enzymes

Research indicates that polyphenols interact with protein-digesting enzymes, inhibiting their enzymatic activity and thereby reducing the digestion and absorption of proteinaceous substances[11]. As observed in Fig. 5, the CMP-LSOPC NPs group effectively inhibits gastric protease during the gastric digestion phase, indicating an inhibition of AGEs hydrolysis in the stomach. CMP exhibits certain promoting effects on gastric protease, enhancing the hydrolysis of glycated proteins. In the gastric phase, the LSOPC and CMP-LSOPC NPs group shows a higher inhibition of trypsin activity, while the CMP group exhibits a lower inhibition. However, during the intestinal phase, the CMP-LSOPC NPs group's inhibitory rate on trypsin activity is significantly higher than that of LSOPC. This could be due to the alkaline environment in the intestine and the more active nature of pancreatic protein, resulting in enhanced inhibitory capacity of the complex.

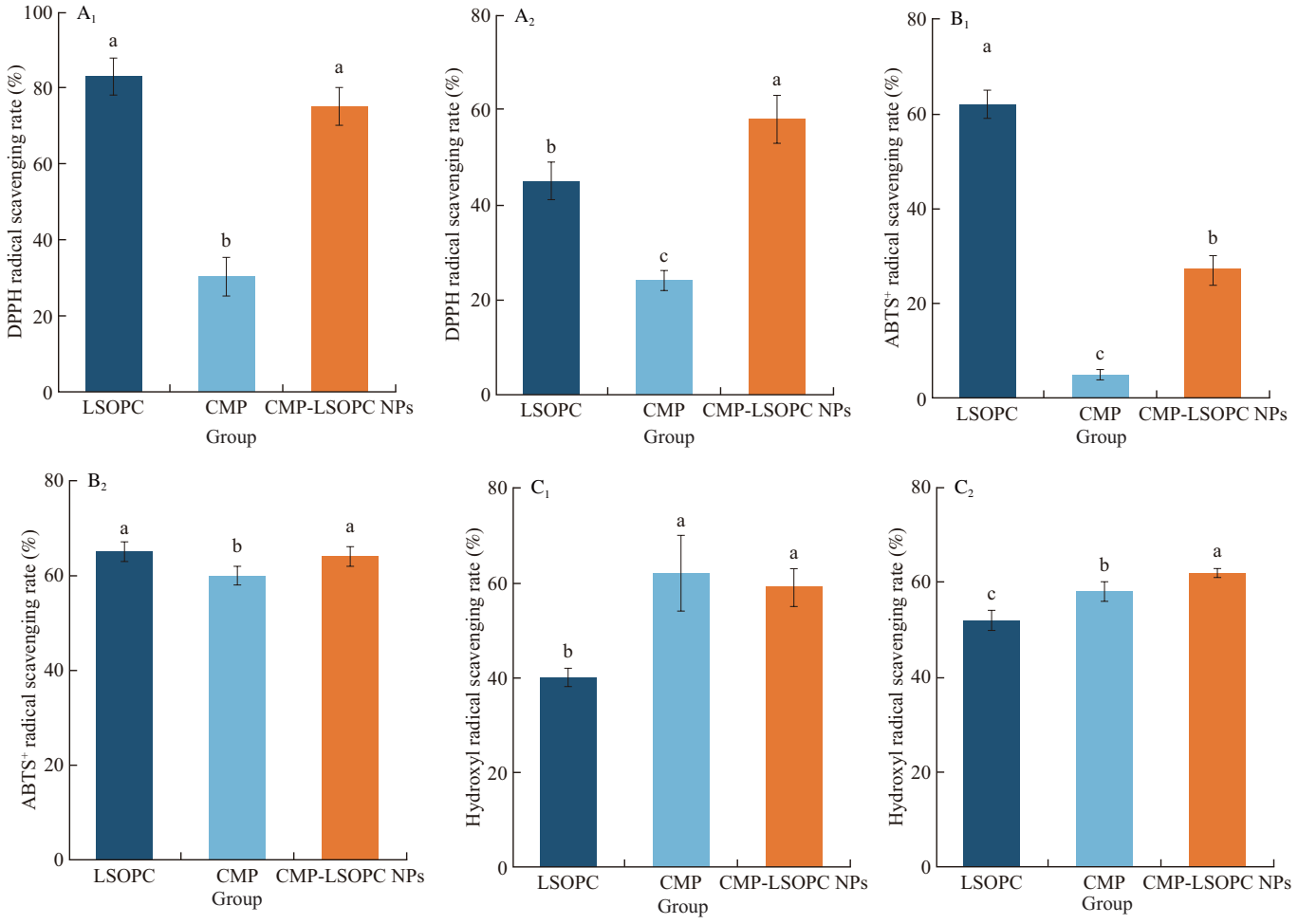

Fig. 4 Antioxidant capacity of digestive fluids.Different lowercase letters indicate significant differences. DPPH radical scavenging rate in (A_1) gastric and (A_2) intestinal; $ABTS^+$ radical scavenging rate in (B_1) gastric and (B_2) intestinal; Hydroxyl radical scavenging rate in (C_1) gastric and (C_2) intestinal. Different lowercase letters indicate significant differences ($P < 0.05$).

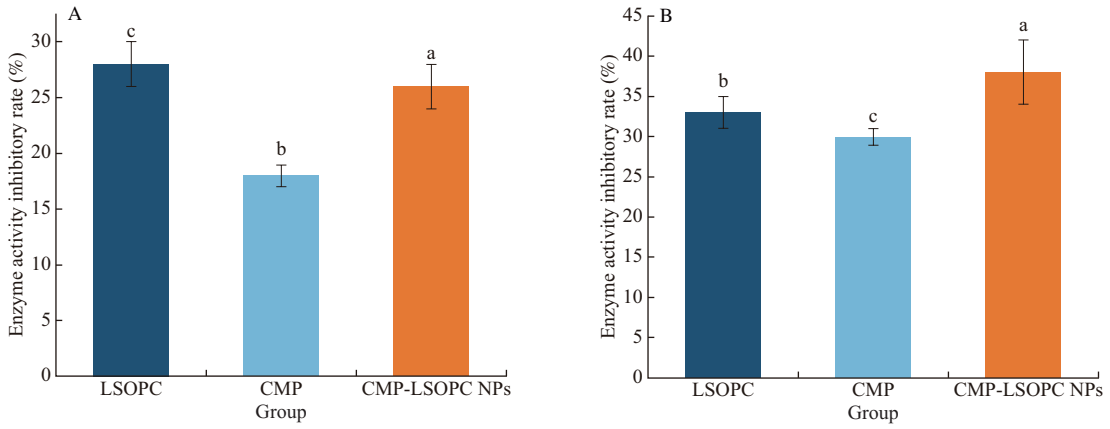

Fig. 5 Impact on digestive enzyme activity in (A) gastric and (B) intestinal. Different lowercase letters indicate significant differences ($P < 0.05$).

The FTIR spectra of the interaction between LSOPC, CMP, CMP-LSOPC NPs, and digestive enzymes are shown in Fig. 6. Changes in the secondary structure of proteins can usually be interpreted through the extension of the amide I band (1 700–1 600 cm^{-1}) and the shift of the amide II band (1 600–1 500 cm^{-1}). FTIR spectra identify changes in protein secondary structures and confirm interactions by monitoring spectral shifts and intensity changes in these 2 bands. The spectra reveal that the addition of LSOPC, CMP, CMP-LSOPC NPs induces changes in these bands. Spectral shifts in the 1 200–1 600 cm^{-1} range suggest enzyme binding to the samples through C=O, C–N, and N–H. Additionally, peak changes at 3 400 cm^{-1} indicate that LSOPC, CMP, CMP-LSOPC NPs primarily form hydrogen bonds with digestive enzymes[34].

The shift in peak positions of participating groups depends on hydrogen bonding or other interactions between different chemical groups. The secondary structural characteristics of the digestive enzymes change significantly after interaction with the samples, possibly due to conformational unfolding and aggregation following reaction with the samples[35].

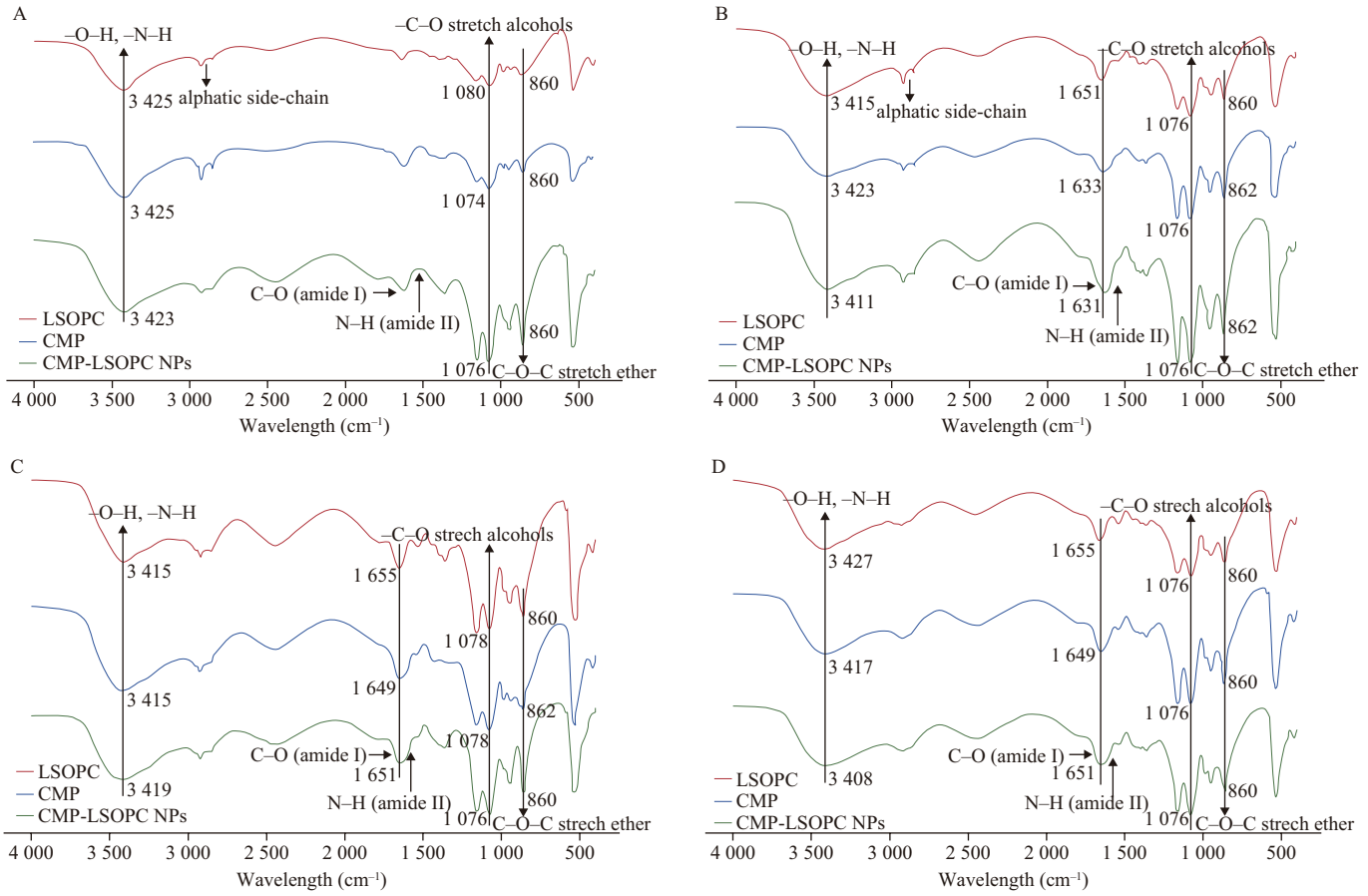

Fig. 6 FTIR spectra under different conditions after sample treatment. (A) Spectra obtained after treatment with gastric protease (pH = 2); (B) spectra after treatment with pancreatic enzyme (pH = 7); (C) spectra of glycated proteins at pH = 2; (D) spectra of glycated proteins at pH = 7. Different lowercase letters indicate significant differences.

Fig. 7 shows the microscopic structural alterations of CMP-LSOPC NPs under enzymatic Interaction. As demonstrated in Fig. 7A, G-CS structures appear as relatively smooth, layered structures. With the addition of LSOPC samples, the intact layered structures fracture, showing holes and fragmentation (Figs. 7B-D and I-K). In the gastric protease group's micrographs (Figs. 7E-H), more pronounced holes and protrusions are observed after the addition of LSOPC and CMP; in the CMP-LSOPC NPs group, more ruptured holes are found. In the pancreatic enzyme group (Figs. 7L-O), LSOPC exhibits a denser structure with noticeable holes and humps, whereas CMP-LSOPC NPs are more fragmented and looser. This suggests an interaction between the samples and proteins, altering the microscopic structure of the proteins.

Therefore, the binding of LSOPC, CMP, and CMP-LSOPC NPs with digestive enzymes through hydrogen bonds and hydrophobic interactions forms complexes, leading to rearrangement of protein peptide chains and consequently inhibiting enzyme activity.

3.4.3 LSOPC remaining rate

As shown in Table 4, the CMP-LSOPC NPs group exhibited higher LSOPC content during the gastric phase compared to LSOPC alone, indicating that CMP protects LSOPC to some degree. During intestinal digestion, the LSOPC content in the the CMP-LSOPC NPs group decreased, compared with the LSOPC group. More LSOPC were depleted in the CMP-LSOPC NPs group in this intestinal stage. Suggesting CMP-LSOPC has higher activity than LSOPC alone, in accord with the results shown in Fig. 4, CMP-LSOPC exhibiting much stronger radical scavenging capability.

Table 4
LSOPC remaining rate (%) after gastric (2 h) and intestinal (4 h) digestions.

Time	LSOPC	CMP-LSOPC NPs	*P* value
2 h	95.13 ± 0.98	99.03 ± 0.49	
4 h	66.07 ± 0.51	53.08 ± 2.52	< 0.01

3.5 Effects of CMP-LSOPC NPs on digestion-derived oligopeptide AGEs

We detected 8 peptide sequences, designated as P1 to P8, as shown in Table 5. Among these, $C_6H_4O_2$ modification (pyrrole modification) is a benzene ring compound modification that can alter the hydrophobicity and charge distribution of the peptide by introducing aromatic rings. Oxidation typically occurs on sulfur-containing amino acids in proteins, altering their oxidation state and affecting protein structural stability and function. Hex modification involves the covalent binding of a peptide with hexose sugars (such as glucose or galactose), a common glycation modification. Hex modifications not only affect the mass-to-charge ratio but may also change the physicochemical properties, such as solubility and stability, of the peptides.

In our analysis, we primarily detected lysine pyrrole modifications (e.g., P1-2, P2-2, P2-3, P2-4, P4-1, P4-2, P6-2, P7) and methionine

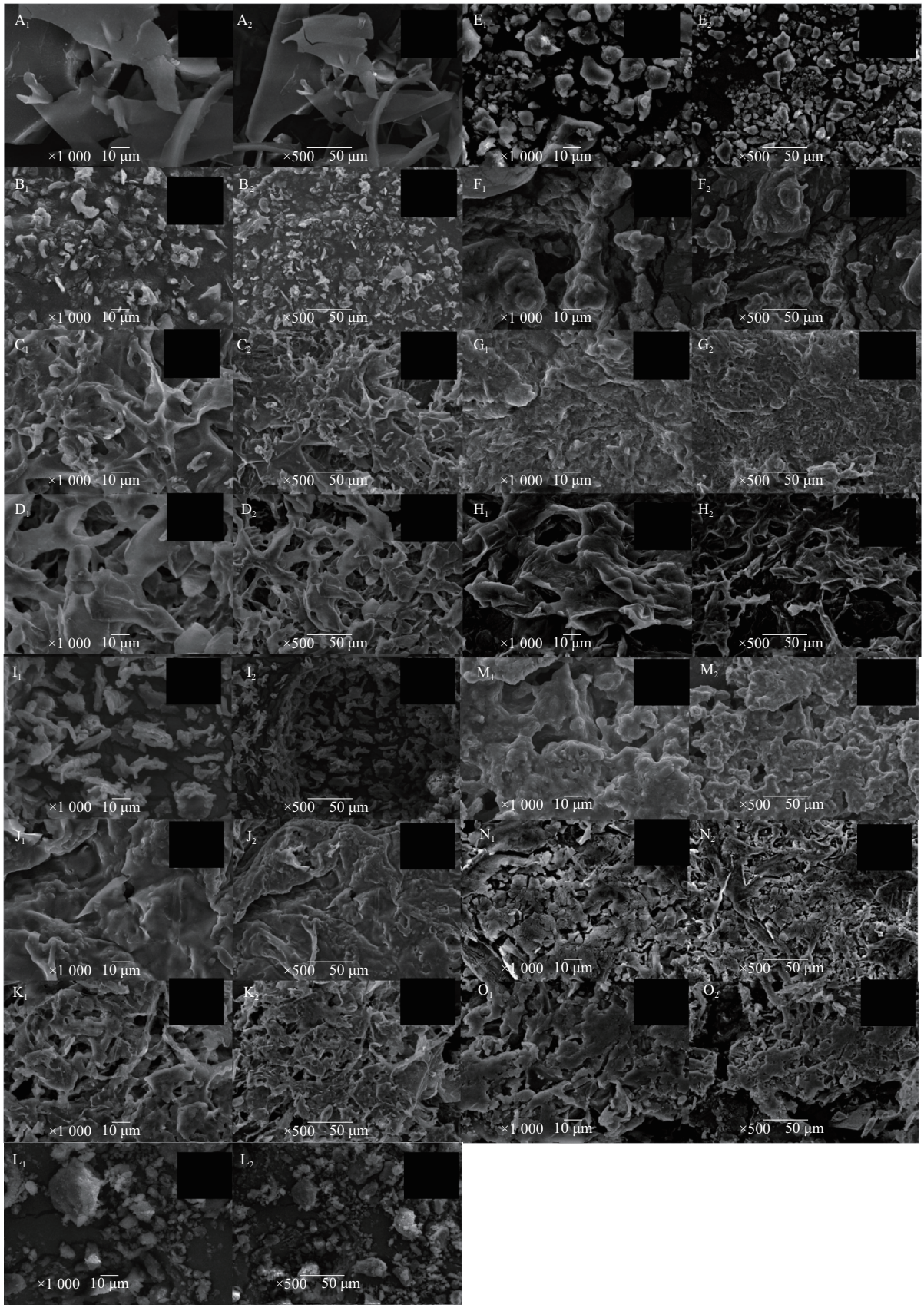

Fig. 7 Microstructural images of the sample-digestive enzyme interactions. (A) G-CS; (B-D) Experimental groups: interactions of LSOPC, CMP, CMP-LSOPC NPs with glycated casein (pH 2); (E) Pepsin control (pH 2); (F-H) Experimental groups: interactions of LSOPC, CMP, CMP-LSOPC NPs with pepsin (pH 2); (I-K) Experimental groups: interactions of LSOPC, CMP, CMP-LSOPC NPs with G-CS (pH 7); (L) Trypsin control (pH 7); (M-O) Experimental groups: interactions of LSOPC, CMP, CMP-LSOPC NPs with trypsin (pH 7). Same letters with different numbers represent images at different magnifications.

Table 5
Summary of protein modification shotgun analysis results based on ESI mass spectrometry technique.

ID	Sequence	Modification	MH+ (Da)	XCorr					
				G-CS		G-CS + LSOPC		G-CS + LSOPC-CMP NPs	
				ETD	HCD	ETD	HCD	ETD	HCD
P1-1	HKEMPFPK	K2(Hex(2))	1 337.634 4	2.05	2.42				2.33
P1-2	HKEMPFPK	K2($C_6H_4O_2$)	1 121.547 6	1.53	3.21			1.23	3.38
P1-3	HKEMPFPK		1 013.527 2		2.40				2.04
P1-4	HKEMPFPK	M4(Oxidation)	1 029.523 5		1.44		1.02		1.23
P1-5	HKEMPFPK	K2(Hex(2)); M4(Oxidation)	1 353.629 6			2.31			
P2-1	EAMAPKHKEMPFPK	M3(Oxidation); K8($C_6H_4O_2$); M10(Oxidation)	1 780.830 8	1.07		1.15		1.26	
P2-2	EAMAPKHKEMPFPK	M3(Oxidation); K6($C_6H_4O_2$); K8($C_6H_4O_2$); M10(Oxidation)	1 888.834 7		1.37				
P2-3	EAMAPKHKEMPFPK	K8($C_6H_4O_2$); M10(Oxidation); K14(Hex(2))	2 088.936 7			3.51	1.93		
P2-4	EAMAPKHKEMPFPK	M3(Oxidation); K8($C_6H_4O_2$); M10(Oxidation); K14(Hex(2))	2 104.931 7			2.68	2.18		
P2-5	EAMAPKHKEMPFPK	K8(Hex); M10(Oxidation); K14(Hex)	1 980.953 4				1.01		
P2-6	EAMAPKHKEMPFPK	K6(C_3H_2O); K8($C_3H_4O_2$); M10(Oxidation)	1 782.917 7				1.70		1.23
P3-1	EMPFPK	M2(Oxidation)	764.367 1		1.75		1.79		1.82
P3-2	EMPFPK		748.372 4		1.63		1.64		1.71
P4-1	IEKFQSEEQ QQTEDELQ DK	K3($C_6H_4O_2$)	2 460.151 3			1.02			
P4-2	IEKFQSEEQ QQTEDELQ DK	K3(Hex); K19($C_6H_4O_2$)	2 622.135 9						1.06
P5	KIEKFQSEEQQQTEDELQDK	K4(Hex); K20(Hex)	2 804.302 9				2.61		
P6-1	VKEAMAPK	M5(Oxidation)	889.466 3				1.04		1.02
P6-2	VKEAMAPK	K2(Hex); K8($C_6H_4O_2$)	1 143.546 3						1.05
P7	EAMAPKHK	M3(Oxidation); K6($C_6H_4O_2$); K8($C_6H_4O_2$)	1 143.520 9				1.03		
P8	FQSEEQQQTEDELQDK		1 981.841 7						1.14

Note: XCorr, cross-correlation, indicates the match quality between observed and theoretical peptide spectra (higher values mean better matches); ETD is a type of MS technique fragmenting peptides by electron transfer to ions, useful for post-translational (PTM) identification; HCD, higher-energy collisional dissociation, is another type of MS technique using high-energy collisions to break peptide bonds, providing detailed peptide sequence and PTM information.

oxidation and Hex modifications (e.g., P1-4, P1-5, P2-1, P2-2, P2-3, P2-4, P2-5, P2-6) (Fig. 8). For instance, in P1-1, the Hex(2) modification results in a mass-to-charge ratio of 1 337.634 40 Da. In HCD mode, this peptide exhibits an XCorr value of 2.42, compared to 2.05 in ETD mode, indicating higher signal matching accuracy in HCD mode. This suggests that HCD activation is more effective in enhancing the ionization efficiency of this peptide, likely due to its superior charge state and dissociation characteristics[36], producing clearer fragmentation patterns. Additionally, P1-2 shows an XCorr value of 1.53 in ETD mode, which significantly increases to 3.21 in HCD mode. This difference reflects how modification types can affect peptide secondary structure, potentially altering its folding[37] and thus affecting mass spectrometric detection efficiency. The data in Table 5 also reveals other modification patterns in P1 and P2 peptides. For instance, P2 peptides exhibit significant physicochemical property changes due to multiple complex modifications, such as $C_6H_4O_2$, oxidation, and Hex(2) (e.g., P2-3 and P2-4). These modifications may alter the charge distribution of the peptides, affecting their ionization and dissociation behavior in mass spectrometry, and potentially influencing their function[36,38]. The detected lysine oxidation and Hex modifications (e.g., P1-1, P1-2, P4-1 and P4-2) are common glycation types that can impact protein function and stability. Samples with the same peptide sequence (e.g., P1, P2, P3, P4 and P6) exhibit different types of modifications, which may result from differences in sample preparation or the inherent heterogeneity of biological samples[39].

Additionally, we differentiated the peptide quantity and length among the 3 samples (G-CS, G-CS + LSOPC, G-CS + LSOPC-CMP NPs). The results showed that G-CS sample, getting most amount of peptides with short chains (Table 5), P1-3 had a higher XCorr value in the G-CS sample. In the G-CS + LSOPC and G-CS + LSOPC-CMP NPs samples, the amount of peptides was relatively lower, and possessing longer chains. P2-3 had the highest XCorr value in the G-CS + LSOPC sample. Specifically, the average peptide length in the G-CS sample was 6 amino acids, whereas the average peptide lengths in the G-CS + LSOPC and G-CS + LSOPC-CMP NPs samples were 12 and 10 amino acids, respectively. The reduction in shorter peptides could potentially reduce the absorption of harmful AGEs[40], which presents a potential health benefit. However, the presence of longer glycated peptides in the gastrointestinal tract, especially in the colon, may pose risks, such as promoting inflammation or disrupting gut microbiota[41]. Further research is needed to explore these potential risks and to balance the benefits of reducing short peptide absorption with the possible adverse effects of longer peptide accumulation.

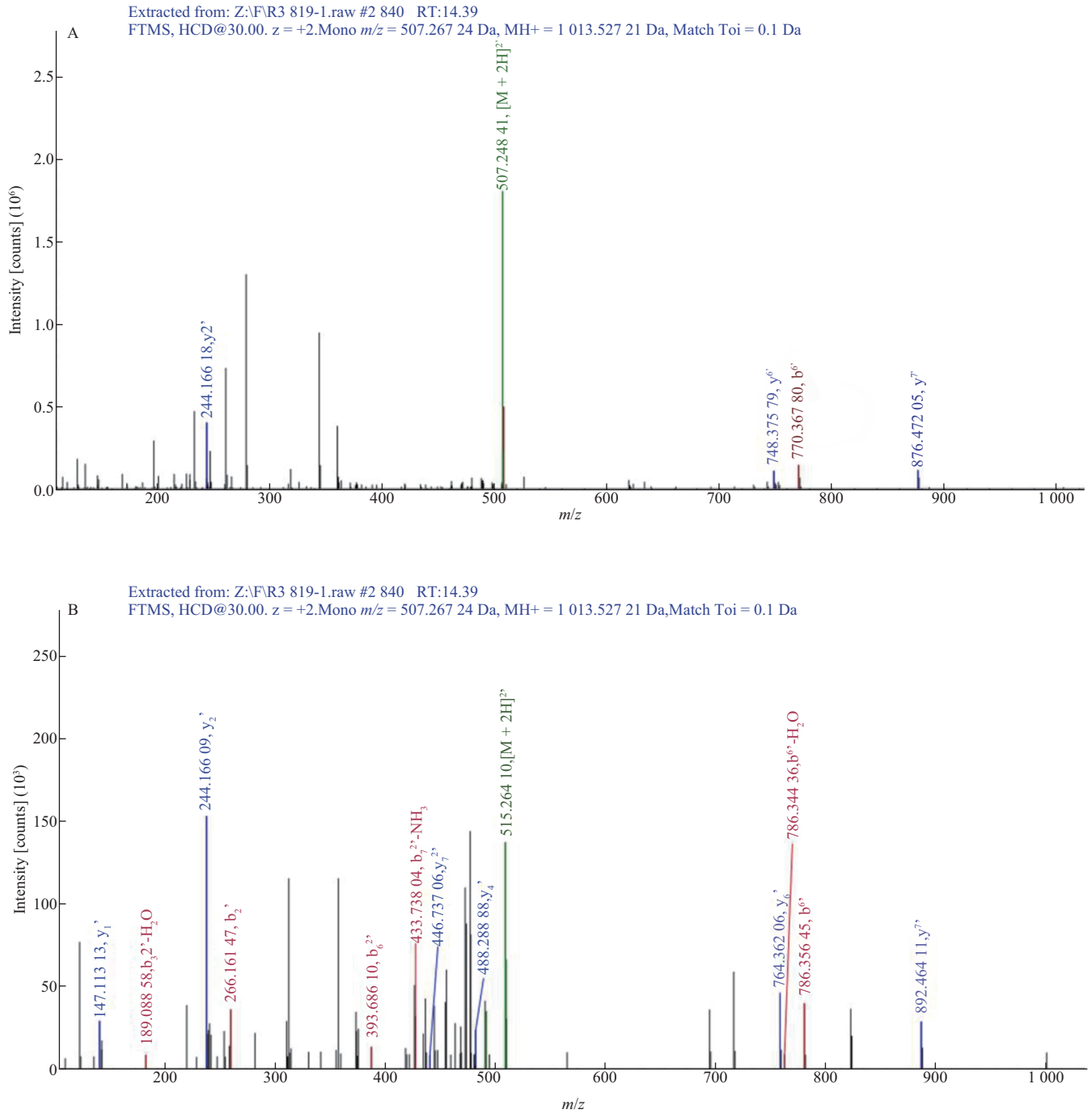

Fig. 8 Representative mass spectra of selected peptides illustrating the impact of modifications and activation types on peptide fragmentation patterns. (A) Mass spectrum of P1-3 as a baseline for comparison; (B) Mass spectrum of P1-4, highlighting changes in mass-to-charge ratio and fragmentation patterns due to the modification; (C) Mass spectrum of P2-1, illustrating the complexity introduced by multiple modifications; (D) Mass spectrum of P6-1, further demonstrating how specific amino acid modifications affect mass spectrometric characteristics.

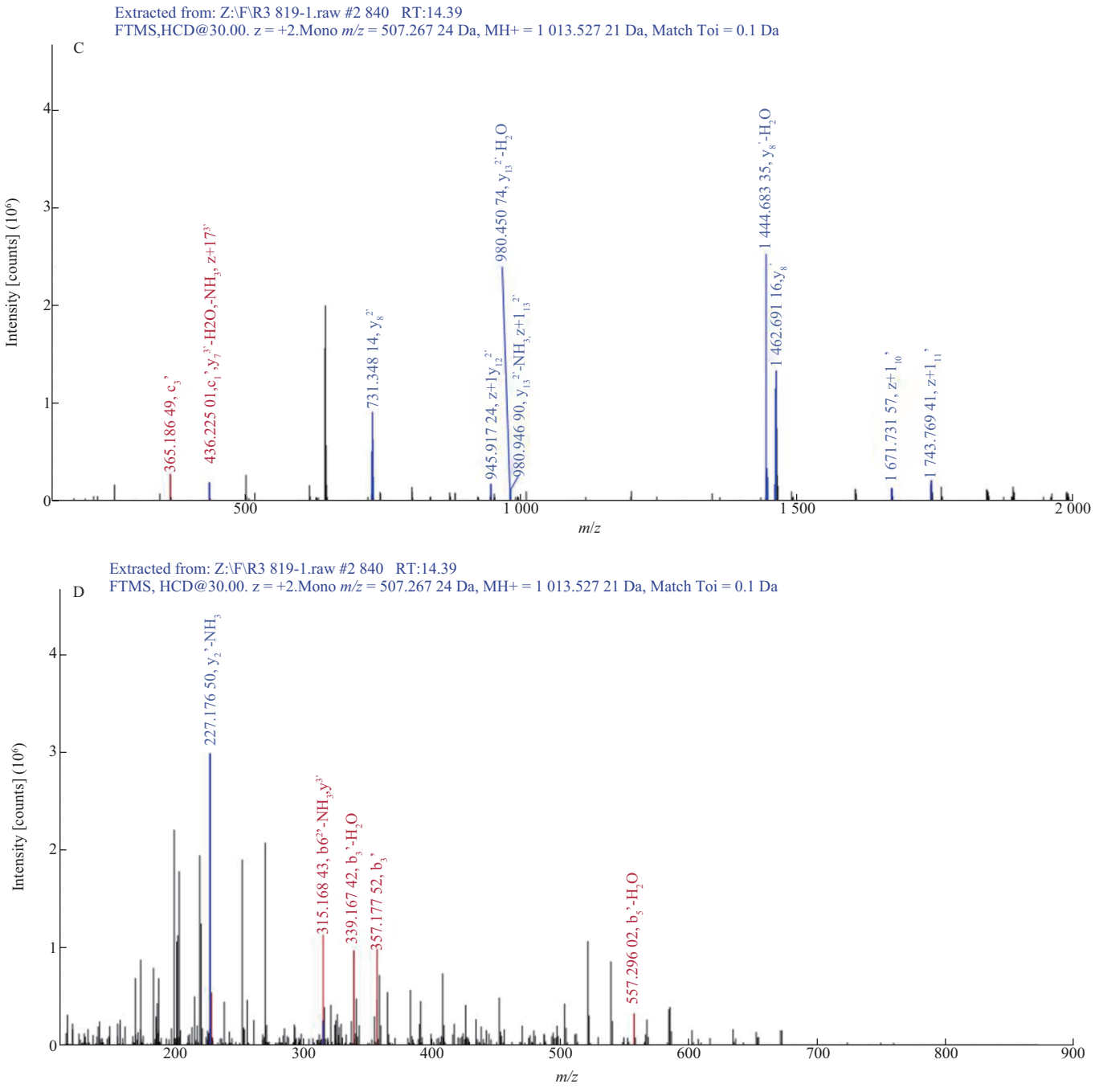

Fig. 8 (*Continued*)

4. Conclusion

In this study, CMP-LSOPC NPs were synthesized and characterized to assess their ability to inhibit AGEs during the digestion process. The general mechanism of this inhibition is illustrated in Fig. 9. It was discovered that the introduction of CMP reduces the degradation of LSOPC, thereby enhancing the stability of LSOPC during gastrointestinal digestion. In the gastric phase, CMP forms aggregates with LSOPC NPs, which protect LSOPC and significantly mitigate its degradation. Furthermore, these aggregates are capable of binding with pepsin, thereby diminishing pepsin activity. During the intestinal phase, the aggregates release LSOPC. The CMP-LSOPC NPs bind to trypsin *via* hydrogen bonds, significantly attenuating trypsin activity and consequently decreasing the content of free AGEs during gastrointestinal digestion. Moreover, the antioxidant capacity of the digestion samples was augmented following the addition of CMP-LSOPC NPs. Therefore, employing CMP as a delivery vehicle for targeted intestinal release of LSOPC can reduce the loss of LSOPC during digestion. Lastly, our oligopeptide analysis revealed that the peptides in the sample groups (G-CS + LSOPC and G-CS + LSOPC-CMP NPs) are generally longer due to reduced digestive enzyme activity, suggesting that they may potentially reduce the absorption of AGEs compared to the control group. This could potentially prevent the absorption of harmful peptides and provide the potential health benefits.

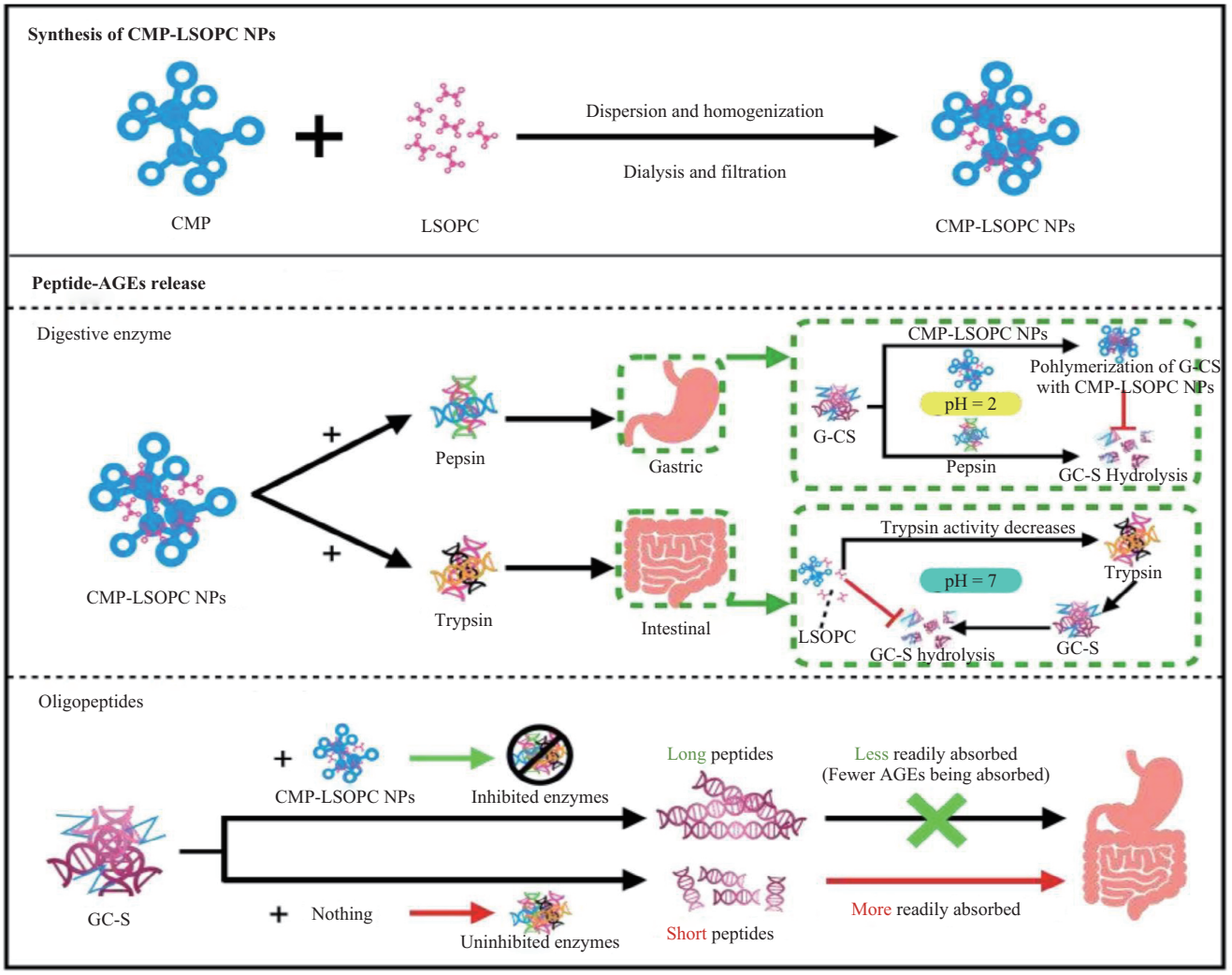

Fig. 9 Mechanism of CMP-LSOPC NPs in inhibiting AGEs release from G-CS during gastrointestinal digestion.

Despite the promising findings and potential benefits of CMP-LSOPC NPs, several limitations must be acknowledged. First, while the reduction in shorter peptides may decrease the absorption of harmful substances such as AGEs, the accumulation of longer glycated peptides could lead to unintended side effects, warranting further investigation. Second, although LC-MS/MS offered valuable insights, the conclusions may be limited by the partial peptide profile presented. The main purpose of this thesis is to focus only on LSOPC modified glycated peptide fragments, and other molecular weight peptides detected by MALDI-TOA or size-rejection method are less focused on our target of this study.

Overall, our findings highlight the potential of CMP-LSOPC NPs in improving the stability and efficacy of LSOPC during digestion, reducing the absorption of harmful shorter peptides, and enhancing the antioxidant capacity of LSOPC. This study provides valuable insights into the development of novel delivery systems for dietary bioactives, for example, adding CMP-LSOPC NPs into wheat flour to make baked bread or cake, contributing to better health outcomes and the sustainable use of natural resources.

Declaration of competing interests

The authors declare that there are no conflicts of interest.

Acknowledgments

This study was supported by the foundation for National Natural Science of China (32472341, 32001705), Hubei Province Science and Technology Personnel Service Enterprise Project (2024DJC019), the Foundation for National Innovation and Entrepreneurship Center for College Students (CSIE) of China (20230100115, 20240200032), the Central Government Guides Local Funds for Scientific and Technological Development (2021BGE045), and Science and Technology Research Project of Education Department of Hubei Province (F2023006).

References

[1] M.N. Lund, C.A. Ray, Control of Maillard reactions in foods: strategies and chemical mechanisms, J. Agric. Food Chem. 65 (2017) 4537-4552. https://doi.org/10.1021/acs.jafc.7b00882.

[2] L. Zhang, P. Wen, J. Zhang, et al., Effects of exogenous advanced glycation end products on oxidative stress and renal injury in healthy mice, eFood 4 (2023) e105. https://doi.org/10.1002/efd2.105.

[3] Y. Nomi, H. Kudo, K. Miyamoto, et al., Free advanced glycation end product distribution in blood components and the effect of genetic polymorphisms, Biochimie 179 (2020) 69-76. https://doi.org/10.1016/j.biochi.2020.09.010.

[4] K. Byun, Y. Yoo, M. Son, et al., Advanced glycation end-products produced systemically and by macrophages: a common contributor to inflammation and degenerative diseases, Pharmacol. Ther. 177 (2017) 44-55. https://doi.org/10.1016/j.pharmthera.2017.02.030.

[5] G. Jia, M.A. Hill, J.R. Sowers, Diabetic cardiomyopathy: an update of mechanisms contributing to this clinical entity, Circ. Res. 122 (2018) 624-638. https://doi.org/10.1161/CIRCRESAHA.117.311586.

[6] P.M. Seferović, W.J. Paulus, Clinical diabetic cardiomyopathy: a two-faced disease with restrictive and dilated phenotypes, Eur. Heart. J. 36 (2015) 1718-1727. https://doi.org/10.1093/eurheartj/ehv134.

[7] V. Rigalleau, N. Foussard, A. Bertrand, et al., Lung cancer and diabetes: a role for advanced glycation end-products? Eur. J. Clin. Invest. 51 (2021) e13389. https://doi.org/10.1111/eci.13389.

[8] J. Wang, M. Zhao, T. Liu, et al., Guidelines for the digestive enzymes inhibition assay, eFood 3 (2022) e31. https://doi.org/10.1002/efd2.31.

[9] F. Lu, Y. Li, B. Zhou, et al., Early-life supplementation of grape polyphenol extract promotes polyphenol absorption and modulates the intestinal microbiota in association with the increase in mRNA expression of the key intestinal barrier genes, Food Funct. 12 (2021) 602-613. https://doi.org/10.1039/d0fo02231d.

[10] Q. Zhang, Y. Wang, L. Fu, Dietary advanced glycation end-products: perspectives linking food processing with health implications, Compr. Rev. Food Sci. Food Saf. 19 (2020) 2559-2587. https://doi.org/10.1111/1541-4337.12593.

[11] Q. Wu, K. Zhao, Y. Chen, et al., Effect of lotus seedpod oligomeric procyanidins on AGEs formation in simulated gastrointestinal tract and cytotoxicity in Caco-2 cells, Food Funct. 12 (2021) 3527-3538. https://doi.org/10.1039/d0fo03152f.

[12] Z. Liang, X. Chen, L. Li, et al., The fate of dietary advanced glycation end products in the body: from oral intake to excretion, Crit. Rev. Food Sci. Nutr. 60 (2020) 3475-3491. https://doi.org/10.1080/10408398.2019.1693958.

[13] J. Wang, M. Bie, W. Zhou, et al., Interaction between carboxymethyl pachyman and lotus seedpod oligomeric procyanidins with superior synergistic antibacterial activity, Carbohydr. Polym. 212 (2019) 11-20. https://doi.org/10.1016/j.carbpol.2019.02.030.

[14] R.L. Prior, E. Fan, H. Ji, et al., Multi-laboratory validation of a standard method for quantifying proanthocyanidins in cranberry powders, J. Sci. Food Agric. 90 (2010) 1473-1478. https://doi.org/10.1002/jsfa.3966.

[15] L.S. Simões, L. Abrunhosa, A.A. Vicente, et al., Suitability of β-lactoglobulin micro- and nanostructures for loading and release of bioactive compounds, Food Hydrocoll. 101 (2020) 105492. https://doi.org/10.1016/j.foodhyd.2019.105492.

[16] R.A. Dixon, S. Sarnala, Proanthocyanidin biosynthesis-a matter of protection, Plant Physiol. 184 (2020) 579-591. https://doi.org/10.1104/pp.20.00973.

[17] L.C. Chen, S.K. Kung, H.H. Chen, et al., Evaluation of Zeta potential difference as an indicator for antibacterial strength of low molecular weight chitosan, Carbohydr. Polym. 82 (2010) 913-919. https://doi.org/10.1016/j.carbpol.2010.06.017.

[18] M.E. Ahmed, H.M. Mohamed, M.I. Mohamed, et al., Sustainable antimicrobial modified chitosan and its nanoparticles hydrogels: synthesis and characterization, Int. J. Biol. Macromol. 162 (2020) 1388-1397. https://doi.org/10.1016/j.ijbiomac.2020.08.048.

[19] S.A. Jin, S.A. Khan, R.J. Spontak, et al., Anion-specific water interactions with nanochitin: Donnan and osmotic pressure effects as revealed by quartz microgravimetry, Langmuir 37 (2021) 11242-11250. https://doi.org/10.1021/acs.langmuir.1c01585.

[20] J. Xie, S. Reverdatto, A. Frolov, et al., Structural basis for pattern recognition by the receptor for advanced glycation end products (RAGE), J. Biol. Chem. 283 (2008) 27255-27269. https://doi.org/10.1074/jbc.M801622200.

[21] A. Brodkorb, L. Egger, M. Alminger, et al., INFOGEST static *in vitro* simulation of gastrointestinal food digestion, Nat. Protoc. 14 (2019) 991-1014. https://doi.org/10.1038/s41596-018-0119-1.

[22] M. Minekus, M. Alminger, P. Alvito, et al., A standardised static *in vitro* digestion method suitable for food-an international consensus, Food Funct. 5 (2014) 1113-1124. https://doi.org/10.1039/c3fo60702j.

[23] I.I. Koleva, T.A. van Beek, J.P. Linssen, et al., Screening of plant extracts for antioxidant activity: a comparative study on three testing methods, Phytochem. Anal. 13 (2002) 8-17. https://doi.org/10.1002/pca.611.

[24] D. Sun, S. Huang, S. Cai, et al., Digestion property and synergistic effect on biological activity of purple rice (*Oryza sativa* L.) anthocyanins subjected to a simulated gastrointestinal digestion *in vitro*, Food Res. Int. 78 (2015) 114-123. https://doi.org/10.1016/j.foodres.2015.10.029.

[25] J.F. Meng, Y.L. Fang, M.Y. Qin, et al., Varietal differences among the phenolic profiles and antioxidant properties of four cultivars of spine grape (*Vitis davidii* Foex) in Chongyi County (China), Food Chem. 134 (2012) 2049-2056. https://doi.org/10.1016/j.foodchem.2012.04.005.

[26] B. Petrat-Melin, P. Andersen, J.T. Rasmussen, et al., *In vitro* digestion of purified β-casein variants A(1), A(2), B, and I: effects on antioxidant and angiotensin-converting enzyme inhibitory capacity, J. Dairy Sci. 98 (2015) 15-26. https://doi.org/10.3168/jds.2014-8330.

[27] R. Gonçalves, S. Soares, N. Mateus, et al., Inhibition of trypsin by condensed tannins and wine, J. Agric. Food Chem. 55 (2007) 7596-7601. https://doi.org/10.1021/jf071490i.

[28] Y. Kong, N. Feng, Y. Liang, et al., Molecular mechanism of lotus seedpod oligomeric procyanidins inhibiting the absorption of oligopeptide-advanced glycation end products, J. Agric. Food Chem. 71 (2023) 12311-12324. https://doi.org/10.1021/acs.jafc.3c04265.

[29] M. Liu, F. Wang, C. Pu, et al., Nanoencapsulation of lutein within lipid-based delivery systems: characterization and comparison of zein peptide stabilized nano-emulsion, solid lipid nanoparticle, and nano-structured lipid carrier, Food Chem. 358 (2021) 129840. https://doi.org/10.1016/j.foodchem.2021.129840.

[30] Z. Wu, J. Ming, R. Gao, et al., Characterization and antioxidant activity of the complex of tea polyphenols and oat β-glucan, J. Agric. Food Chem. 59 (2011) 10737-10746. https://doi.org/10.1021/jf202722w.

[31] C. Iannuzzi, G. Irace, I. Sirangelo, Differential effects of glycation on protein aggregation and amyloid formation, Front. Mol. Biosci. 1 (2014) 9. https://doi.org/10.3389/fmolb.2014.00009.

[32] Q. Wu, Y. Kong, Y. Liang, et al., Protective mechanism of fruit vinegar polyphenols against AGEs-induced Caco-2 cell damage, Food Chem.: X 19 (2023) 100736. https://doi.org/10.1016/j.fochx.2023.100736.

[33] Q. Wu, Y. Liang, Y. Kong, et al., Role of glycated proteins *in vivo*: enzymatic glycated proteins and non-enzymatic glycated proteins, Food Res. Int. 155 (2022) 111099. https://doi.org/10.1016/j.foodres.2022.111099.

[34] D. Yang, S. Gao, H. Yang, Effects of sucrose addition on the rheology and structure of iota-carrageenan, Food Hydrocoll. 99 (2020) 105317. https://doi.org/10.1016/j.foodhyd.2019.105317.

[35] M. Shi, L.Y. Huang, N. Nie, et al., Binding of tea catechins to rice bran protein isolate: interaction and protective effect during *in vitro* digestion, Food Res. Int. 93 (2017) 1-7. https://doi.org/10.1016/j.foodres.2017.01.006.

[36] N.M. Riley, M.J. Rush, C.M. Rose, et al., The negative mode proteome with activated ion negative electron transfer dissociation (AI-NETD), Mol. Cell. Proteomics. 14 (2015) 2644-2660. https://doi.org/10.1074/mcp.M115.049726.

[37] J.N. deGruyter, L.R. Malins, P.S. Baran, Residue-specific peptide modification: a chemist's guide, Biochemistry 56 (2017) 3863-3873. https://doi.org/10.1021/acs.biochem.7b00536.

[38] L.A. Macias, I.C. Santos, J.S. Brodbelt, Ion activation methods for peptides and proteins, Anal. Chem. 92 (2020) 227-251. https://doi.org/10.1021/acs.analchem.9b04859.

[39] S.A. Byrne, M.J. Bedding, L. Corcilius, et al., Late-stage modification of peptides and proteins at cysteine with diaryliodonium salts, Chem. Sci. 12 (2021) 14159-14166. https://doi.org/10.1039/d1sc03127a.

[40] Y. Mashima, K. Horibe, I. Oshiba, et al., Studies on the absorption of 'small peptides' and free amino acids in elemental diets, Clin. Nutr. 3 (1984) 17-21. https://doi.org/10.1016/S0261-5614(84)80017-5.

[41] P.N. K. Nguyen, B.A. McNeill, K. Aston-Mourney, et al., Advanced glycation end-products and their effects on gut health, Nutrients 15 (2023) 405. https://doi.org/10.3390/nu15020405.